Tunable Dual-Band Ultrasensitive Stereo Metamaterial Terahertz Sensor

PENGFEI CAO [1], YUYAO WU[1], ZELONG WANG [1,2], YUAN LI[1], JING ZHANG[1], QIANG LIU[3,4], LIN CHENG [1], AND TIAOMING NIU[1]

[1]School of Information Science and Engineering, Lanzhou University, Lanzhou 730000, China
[2]School of Precision Instruments and Optoelectronics Engineering, Institute of Laser and Optoelectronics, Tianjin University, Tianjin 300072, China
[3]School of Energy and Power Engineering, Nanjing University of Technology, Nanjing 210094, China
[4]Northwest Industries Group Company, Ltd., Xi'an 710043, China

Corresponding authors: Pengfei Cao (caopf@lzu.edu.cn) and Lin Cheng (chenglin@lzu.edu.cn)

ABSTRACT To overcome the effect of analyte thickness and limitation of single wavelength sensing, we propose an ultra-sensitive stereo metamaterial biosensor with double resonance frequencies based on coupling electric resonance and magnetic resonance. The electromagnetic analysis demonstrates that the double resonance coupling, induced by the stereo double-layer structure, can significantly improve sensitive biosensing at the terahertz frequency. The results show that by changing the size of the structure, each resonance frequency can be independently tuned in the range of 0.5-1.8 THz and the maximum refractive index sensitivity is 930.4 GHz/RIU. These results have significant implications for the detection of samples with different frequency points. The proposed ultra-sensitive stereo metamaterial structure has excellent potential for application in biomolecule detection and differentiation.

INDEX TERMS Magnetic resonance, electric resonance, sensitivity, terahertz metamaterial sensing.

I. INTRODUCTION

Among various optical sensing methods, terahertz (THz) spectroscopy (0.1–10 THz) is considered as one of the most promising tools for biological sensing, since the fingerprint vibrational frequency of most chemical and biological molecules (protein, RNA, and DNA) lies in this spectral region [1]–[3]. Moreover, terahertz frequency has many unique advantages in biological detection. The energy of THz photons is low, thus minimizing the damage to biological substances [3], [4]. Therefore, terahertz spectroscopy enables non-contact, non-destructive and unlabeled optical sensing for the study of chemical samples and small biomolecules. However, it is hard to be processed by electronic technology because the terahertz frequency is too high, while its photon energy is too low [1], which causes terahertz biosensing to have limitations in detecting trace biochemicals. Therefore, metamaterials have been developed that significantly

The associate editor coordinating the review of this manuscript and approving it for publication was Chao Zuo [ ].

increase the intensity of the interaction between the analyte and the incident THz wave, thus allowing for higher sensitivity and SNR values [2]–[4]. This is because the introduction of metamaterial resonance causes a significant increase in induced current and magnetic moment [5]. Since the introduction of metamaterials, after years of vigorous development, a large number of theoretical and modelling results have been proposed [6]–[14]. At present, the application of metamaterials is very extensive, and the technology combined with microfluidics has been applied to the detection of biomolecules [2], [10], [15], [16].

These promising sensing tasks are typically achieved by measuring the difference in the resonance response of the metamaterial [17]–[20]. When the analysis sample is overlaid on top of the metamaterial, the altered resonance response is converted into a significant change in the transmitted or reflected signal in the response spectrum, then these changes can be detected directly [18], [21]. This is an effective method for determining the nature of an analytical sample [17], [22]. In order to achieve this principle, many

terahertz metamaterial biosensors with biodetection capabilities have been proposed. The original metamaterials were designed as planar structures that are easy to fabricate. The split ring resonator (SRR) is one of the original designs of strong artificial electromagnetic materials in which each SRR consists of two concentric open loops with opposite openings [23]. This requires a higher sensitivity of the sensor as the samples being detected become more and more microscopic. In order to improve sensitivity or quality factor, many planar structures have been proposed, and some studies have introduced Fano resonance or more complex planar structures [24]–[29]. However, the study of these metamaterial structures is limited by planar structures, which can only introduce electrical or electrical responses. This can increase the dielectric loss and thus decrease its sensing potential. Since the magnetic response caused by the magnetic excitation is very weak or hardly present, the performance of the planar structure cannot be greatly improved. In addition, when the analyte thickness reduces to a few nanometers, the shift in the resonance frequency becomes too small to be detected due to the reduced strength of light-matter interaction. To make effective use of the sensing capability of metamaterial sensors at terahertz frequencies, a large thickness of the analyte is generally desired. However, this can cause the amplitude of the resonance to become very weak, making it difficult to be detected in a noisy environment. To address this problem, the three-dimensional structure came into being. The three-dimensional structure that lifts the split ring from the substrate can greatly reduce the dielectric loss introduced by the substrate, and the three-dimensional structure produces a strong fundamental resonance excited by a pure magnetic field [18]. The performance of this structure is much higher than that of a planar SRR sensor. In recent years, vertical SRR (VSRR) structure has been proposed and analyzed, and many research teams have made various major breakthroughs in the study of vertical structures [18], [24], [30]–[34]. However, most of these three-dimensional structures have only one transmission dip, which may limit the application of sensors in miniaturized and multi-functional optical devices. Recent studies show that multiband sensors are essential for frequency selective detection with reduced environmental disturbance and enhanced detection accuracy [33]. Hence, the three-dimensional THz metamaterial biosensors with multiple resonance modes are in critical need of development.

In this study, we present an ultra-high sensitivity stereo dual-split ring resonator (SDSRR) metamaterial biosensor with two transmission dips (resonance frequencies), where each dip can be independently tuned at 0.5-1.8 THz. This plays an important role in solving the practical problems of microscopic thick samples with different frequency points. In particular, the structure after the planar structure is lifted from the substrate not only introduces magnetic excitation, but also couples the electric resonance by the split ring on the substrate. Hence, the sensitivity of the sensor is greatly improved. This is the main reason why the SDSRR sensor has much higher sensitivity than the VSRR structures.
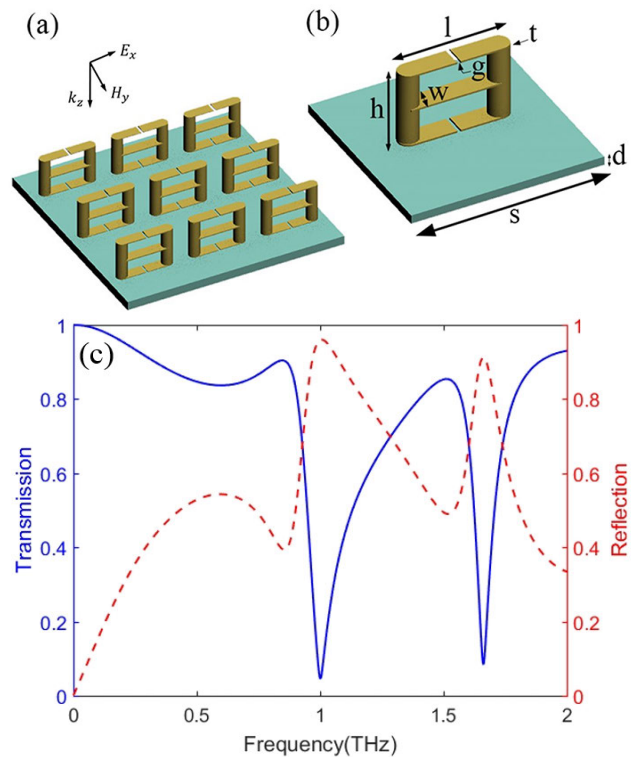
FIGURE 1. (a). Schematic diagram of the arrayed SDSRRs on polyimide substrate. (b). Typical dimensions of samples for unit cell of SRRs: l = 50 μm, w = 12 μm, g = 2 μm, t = 1.5 μm, h = 33 μm. (c). The transmission and reflection spectra of SDSRR.

II. GEOMETRIC STRUCTURE AND METHOD

Figure 1 illustrates the structure of the SDSRR biosensor, and the amplified view of a single unit cell used in the simulation. The incident electromagnetic wave is perpendicularly irradiated on the upper surface of the metamaterial structure along the z-axis of the coordinate system, as shown in the inset of Figure 1(a). The E field is perpendicular to the gap of the SRR array along the x-axis and the H field passes through the SDSRR vertically. The period of the square unit cell used for the simulation is s = 70 μm, as shown in Figure 1(b). The metal structure is made of aluminum, which is built on top of a polyimide substrate, and the numerically calculated substrate thickness is d = 40 μm. This structure has two slots on the top and bottom metal plates, and the width of the two slots is equal to g = 2 μm, and the middle metal plate has no slots. The length and width of the three metal plates (top, middle and bottom) are l = 50 μm and w = 12 μm, respectively, and the thickness of the three metal plates is t = 1.5 μm. The three metal plates are equally spaced by two metal cylinders with a height of h = 33 μm and a diameter of D = 12 μm. The numerical calculations are performed using the frequency domain solver of the commercial EM wave solver CST Microwave Studio (software version is 2014). As seen from the transmission spectrum of the SDSRR, the structure has two transmission dips (resonance frequencies) at 0.990 THz and 1.632 THz, respectively, as shown in Figure 1(c).

Considering the complexity of manufacturing SDSRR structures, according to the effective medium theory, the S-parameter inversion method [35]–[39] can be used to characterize the equivalent refractive index of the artificial structure. At a given frequency, any material that supports only one propagating mode will generally exhibit a well-defined refractive index n, whether the material is continuous or not. However, as the reflection is strong at given frequencies, the impedance matched condition is not satisfied. It means that the impedance z, which is calculated based on S-parameter retrieval methods, is ambiguous, and it is not possible to assign intrinsic values for ε and μ [38], [39]. Furthermore, metal metamaterial structure is not good for transparency and the loss of conductive components needs to be considered [40]. From Figure 1(c), it can be found that reflectivity and transmittance do not add up to 1 at resonance frequencies due to the loss. The loss can be observed through the imaginary part of the effective refractive index Im(n). Here, the refractive index n can be expressed as [35], [36], [39]:

$$n = \frac{1}{kh} \cos^{-1}\left[\frac{1}{2S_{21}}(1 - S_{11}^2 + S_{21}^2) + 2\pi m\right],$$
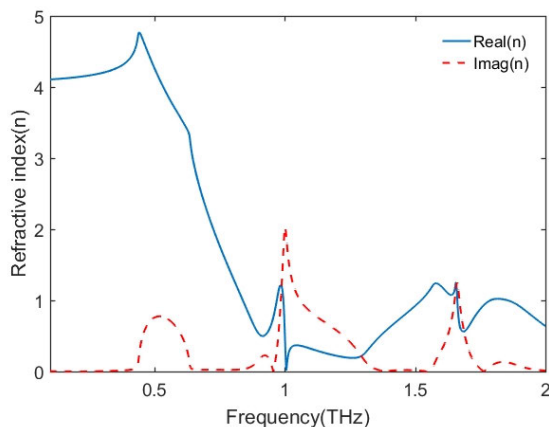$$m = 0, \pm 1, \pm 2, \cdots \tag{1}$$

FIGURE 2. Retrieval effective refractive index *n*.

The effective refractive index n of SDSRR is shown in Figure 2. At 0.990 THz and 1.632 THz, the imaginary part of refractive index Im(n) reaches the maximum, which means there is maximum loss. Obviously, the corresponding equivalent refractive index model based on S-parameter inversion method is found to be in good agreement with transmission dips based on CST software at 0.990 THz and 1.632 THz.

It is well known that when the electric field (E) is parallel to the side containing the SRR gap or when the magnetic field (H) has a component perpendicular to the plane of the ring, the incident electromagnetic radiation can be resonantly coupled to the LC resonance of the SRR by an electric or magnetic field [41]. Therefore, the structure proposed by us can be simply equivalent to the LC circuit diagram. Here, the upper and lower gaps in the structure can be equivalent
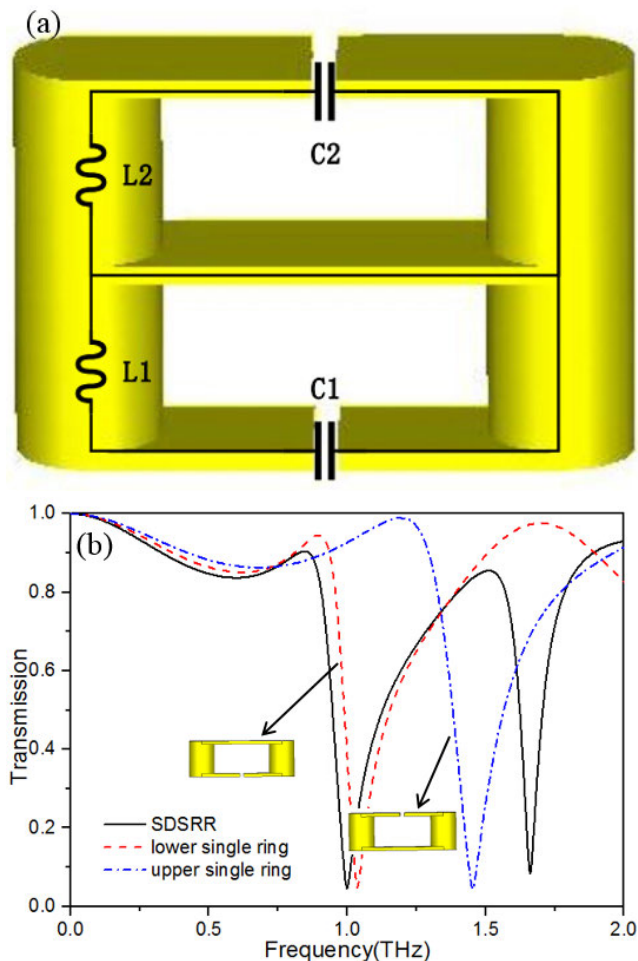
FIGURE 3. (a) Equivalent circuit diagram of SDSRR unit; (b) The transmission spectra of lower ring and upper ring.

to capacitance, and other parts of the metal structure can be equivalent to inductance, as shown in Figure 3(a). According to the equivalent circuit model, Equation (2) is a widely accepted method for qualitatively describing the position of the LC resonance [42]:

$$\omega_{LC} \propto \frac{1}{\sqrt{LC}} \tag{2}$$

Compared with previous work [18], the metal slab is added between the top gap (Tgap) and bottom gap (Bgap) in our structure. As a result, the equivalent circuit is changed. This kind of structure forms two loops, as shown in Figure 3(a). Each loop has its own LC resonance. This is the reason that there are two transmission dips in the transmission spectra. In this case, the SDSRR structure is approximately equivalent to stacking the upper and lower single rings. As shown in Figure 3(b), when there is only the lower single ring, there is a transmission curve at low frequencies, and when there is only the upper single ring, a transmission curve appears at high frequencies. Therefore, the resonance frequencies of upper and lower single rings can be expressed by Equation (3)

through the equivalent circuit model:

$$f_i = \frac{1}{2\pi\sqrt{L_i C_i}} \quad (3)$$

where i is 1 or 2 represents the resonance frequency of the lower single ring or the upper single ring, respectively.

The numerically calculated SDSRR transmission spectrum is shown in Figure 3(b). Two transmission dips (resonance frequencies) are located at 0.990 THz and 1.632 THz, respectively. However, the transmission dips of the upper and lower single ring are 1.032 THz and 1.445 THz, respectively (in the Supplementary documentation, the effective refractive index n of the upper and lower single ring are calculated based on S-parameter retrieval methods). Obviously, the transmission dips of single rings do not overlap with that of SDSRR here. This is due to the coupling effect of the superposition of the double rings, which causes the transmission dips of the single ring and the double rings to shift slightly. Compared to the resonance frequencies of the lower and upper single ring, the resonance frequency of SDSRR has a slight red shift at low resonance frequency, while the resonance frequency of SDSRR has a slight blue shift at high resonance frequency. The reason is that not only does more plasmon field permeate into the substrate in the case, which increases the dielectric loss, but also a part of the photon energy from the lower ring is coupled into that of the upper ring due to the metal slab between the top Tgap and Bgap in SDSRR structure. Thus, lower ring photon energy of SDSRR is smaller than that of lower single ring, as shown in Figure 4a and 4c. As is known, the decrease in photon energy leads to the red shift. Therefore, there is a slight red shift at low resonance frequency. In contrast, the photon energy of the upper ring is enhanced at high resonance frequency. From Figure 4b and 4d, it can be found that a part of the photon energy from the lower ring is coupled into that of the upper ring in the same way. Therefore, upper ring photon energy of SDSRR is more than that of upper single ring, leading to a slight blue shift at high resonance frequency. Thus, we can introduce a coupling coefficient k_i, to express the frequency of the two transmission dips after coupling, respectively:

$$f_1' = f_1 + k_1 * f_2$$
$$f_2' = f_2 + k_2 * f_1 \quad (4)$$

In Equation (4), k_1 represents the attenuation coefficient of the upper ring to the lower ring, and k_2 represents the enhancement coefficient of the lower ring to the upper ring. As the surrounding medium of the upper ring is air and the lower ring contacts the substrate, k_1 is not equal to k_2.

To better explore the coupling resonant mechanism of SDSRR, current distributions of the double rings are compared with that of the single ring, as shown in Figure 4e-h. It can be seen from the figure that whether in the single ring or in the double rings, the current is mainly concentrated on the lower ring close to the base at the low resonance frequency. Correspondingly, most of the current is concentrated on the upper ring at the high resonance frequency. Therefore,
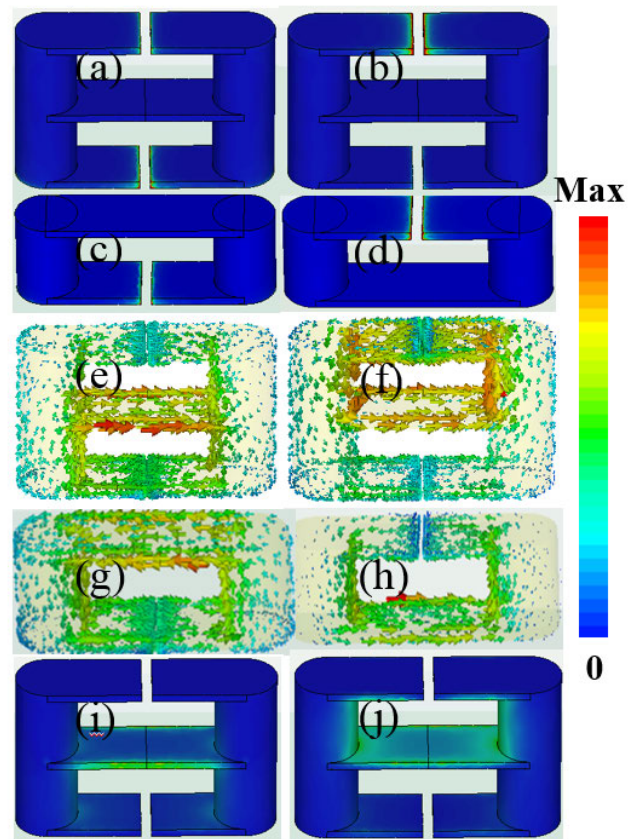
FIGURE 4. (a), (b), (e), (f), (i), (j) are the electric energy density, surface current and magnetic energy density of SDSRR at two resonance points, respectively. (c), (d), (g), (h) are the electric energy density and surface current of the single lower ring and single upper ring, respectively.

the trend of current distributions of the single lower ring and the single upper ring is similar to that of low and high resonance frequency at the double ring structure. This further verifies that the lower ring and the upper ring of the double ring unit are approximately equivalent to stacking the upper and lower rings. Also, the strength of the lower ring is much lower than the strength of the upper ring, as shown in Figure 4e-g. This is because, in our design, it is considered that placing the upper ring on the upper portion can reduce plasma penetration into the substrate and reduce the dielectric loss caused by the substrate. At the same time, a part of the energy from the lower ring is also coupled into that of the upper ring. It further confirms our previous analysis. It is well known that the LC resonance of the SRR can be activated through either an electric-coupling-induced capacitance response or a magnetic-coupling-induced inductance response [43]. The bianisotropy in the lower and upper single rings is introduced due to their asymmetric structures [44]. It is well established that the SRR is intrinsically bianisotropic owing to the absence of inversion symmetry in the structural plane [45]. As displayed in the insets of Figure 3b, symmetry breaking occurs in the lower and upper single ring structures along the incidence direction of the EM wave, which introduces the

bianisotropy. When the EM wave is polarized as indicated in Figure 1a, both the electric and magnetic field components can excite the LC resonance in the lower single ring, upper single ring and SDSRR structures, which introduces a strong bianisotropy effect. Especially for the SDSRR, the magnetic field plays a predominantly important role in high resonance frequency, but electric excitation can also work at low resonance frequency due to coupling effect of the metal slab between the Tgap and Bgap (a circular magnetic current will appear which excites the electric resonance at Bgap), as shown in Figure 4i and 4j. In this case, the resonance caused by the lower ring is electric resonance. Correspondingly, the resonance caused by the upper ring is magnetic resonance. Therefore, these two resonant frequencies can not only be separately adjusted by different gaps of the upper and lower rings, respectively, but can also render good sensing performance. Compared with other VSRR, SDSRR has a unique coupling characteristic.

III. RESULTS AND DISCUSSION

A. TUNABLE

Considering the influence of the geometric structure, the transmission spectrum changes caused by the upper and lower gaps are discussed here. The simulation calculation when the position of the lower gap is constant and the size of the upper gap changes gradually is shown in Figure 5(a). At this time, the low-frequency dip does not move significantly in the transmission spectrum, while the high-frequency dip shows a significant blue shift. From formulas (2) and (3), it can be seen that when the upper gap gradually increases and the capacitance gradually decreases, that is, f_2 gradually increases, and f_1 is basically unchanged. Therefore, f_2' gradually increases. As f_1' is the attenuation factor under the effect of k_1, it is basically unchanged. On the contrary, the simulation calculation when the position of the upper gap is constant and the size of the lower gap changes gradually is shown in Figure 5(b). The low-frequency dip shows a clear blue shift in the transmission spectrum, while the high-frequency dip also has a relatively weak blue shift. Similarly, according to formulas (3) and (4), when the lower gap gradually increases, the capacitance gradually decreases. That is, f_1 gradually increases, and as a result, f_1' gradually increases. Moreover, f_2 basically does not change, but f_2' slightly increases due to the effect of enhancement coefficient k_2. Therefore, the proposed SDSRR structure has good adjustability. By changing the size of the gap in the structure, it can move freely in the range of 1.4-1.8 THz, and the transmission rate exceeds 90%. This further proves that by adjusting the size parameters of the upper and lower metal rings of the double ring unit, the two resonance frequency points of the unit can be adjusted separately.

B. INCIDENT ANGLE

Figure 6 shows the change in the LC resonance transmission spectrum of SDSRR under TEM illumination. Here, the angle
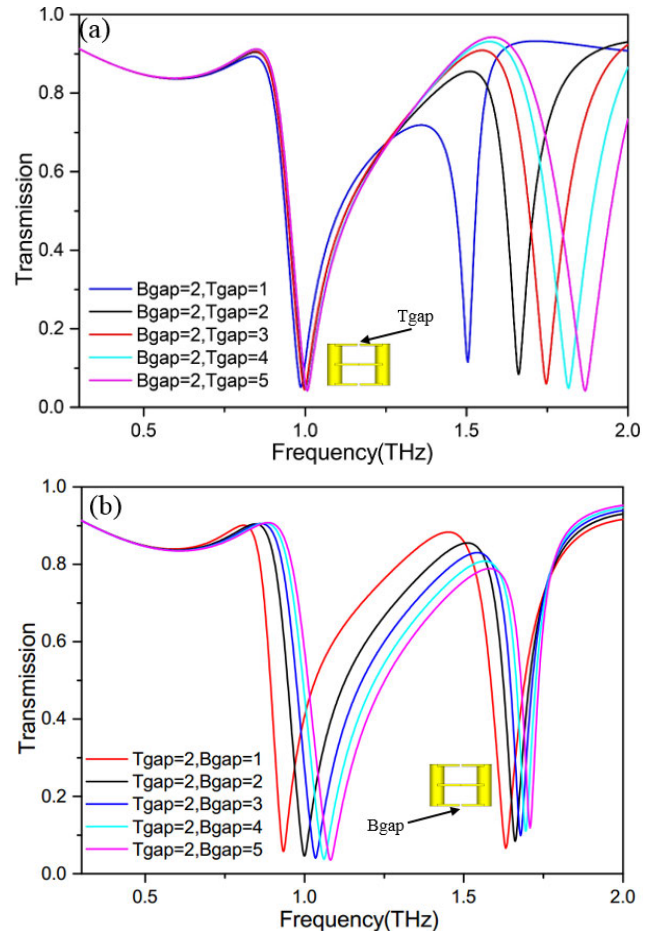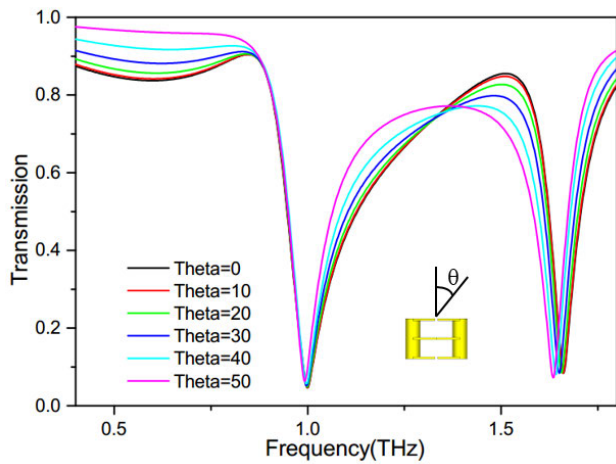
FIGURE 5. The simulated results with different gaps: Transmission spectrum of the size change of the top (a), and bottom gap on the structure(b), respectively.

of incidence increases from 0° to 50°, and the step angle of the incident angle scan used in the simulation is 10°. This figure shows that the spectral characteristics can remain near the resonance position relative to a wide range of incident angles, even up to 50°. As the angle of incidence increases, the transmission curve shows a slight red shift. Through the simulation calculation, it is found that the sensitivity is barely affected by the change in incident angle, indicating that the sensor is not sensitive to the incident angle.

C. SENSITIVITY ASSESSMENT

In order to demonstrate the sensitivity of SDSRR sensor to refractive index, we established the corresponding simulation models and evaluated the performance of SDSRR-based metamaterial sensors. The geometrical parameters of SDSRR sensor are shown in Figure 1. As mentioned earlier, lifting the metamaterial off the plate can introduce stronger resonances, which can be used to detect thicker analytes. First, the relation between the thickness of analytes and shift of resonance frequency is discussed. It is assumed that the refractive index n of the analyte is 1.6, and the transmission spectrum with different thicknesses is shown in Figure 7(a). Its displacement
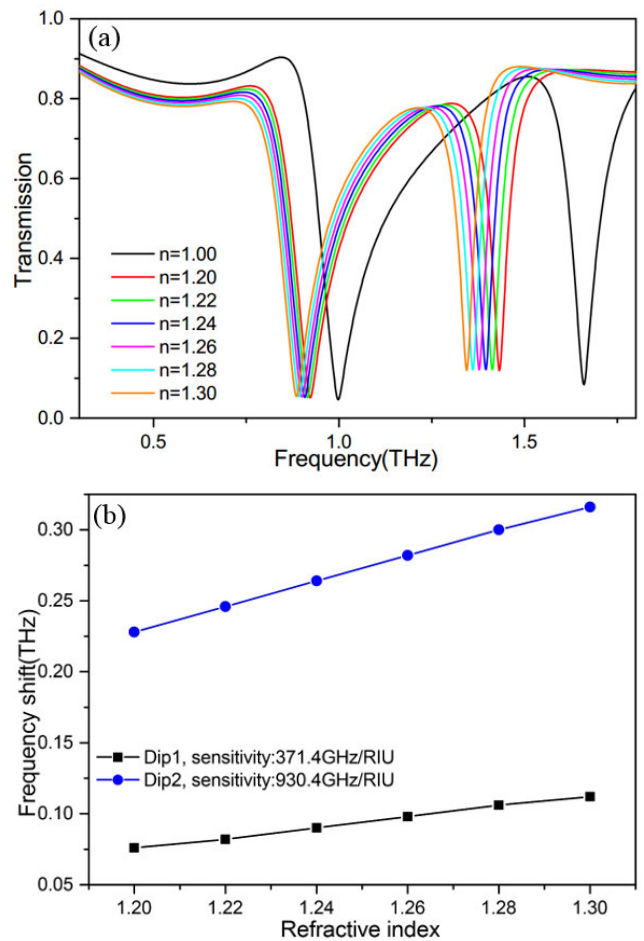
FIGURE 6. The simulated results with different incident angles: Transmission spectral comparison for incidence radiation with increasing incidence angles with a step of 10°.
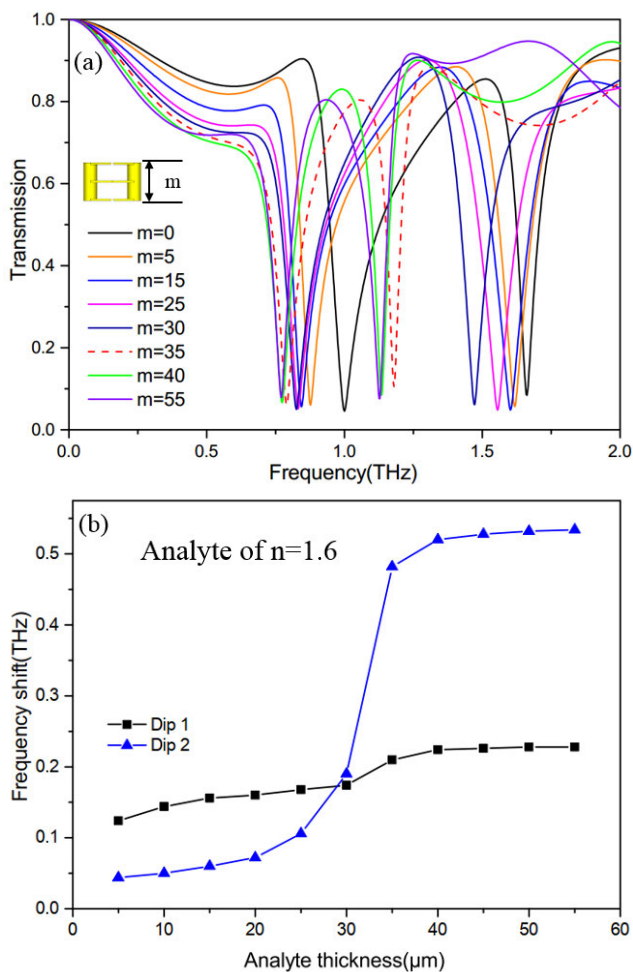
FIGURE 7. The simulated results with different thickness of analytes m: (a) The transmission spectra of the SDSRR with and without analyte overlaid on the sensor. (b)The fitting function using the data of two dips.

relative to the resonance frequency point without analyte is plotted in Figure 7 (b). It can be seen from this figure that when the thickness of the analyte is consistent with the height

of the lower ring, the frequency change caused by the lower ring is greater than that of the upper ring, which is also consistent with our previous theory. Only when the thickness of the analyte is higher than that of the sensor, that is, when the analyte is 35μm, the larger frequency shift of dip 2 can be clearly seen, as shown by the red dash line in Figure 7 (a), and the blue line in Figure 7 (b). When the analyte is higher than the sensor, it can be seen the shift of dip1 is also slightly enhanced due to the coupling effect of the upper ring and the lower ring from formula (3). When the thickness exceeds 50μm, the shift of two dips tends to be stable. After the above discussion, it is assumed that the thickness of the analyte added to the sensor is 50μm, and the refractive index of the environment can be changed. When the refractive index of the environment changes slightly, the transmission spectrum of the sensor changes drastically, as shown in Figure 8.

FIGURE 8. The simulated results which could guide the design of the structure of THz metamaterials biosensor chip. (a). Transmission spectra of SDSRR at different refractive indices; upper and lower gaps are 2μm. (b). The sensitivity of SDSRRs for Dip 1 and Dip 2.

For refractive index sensing, the simulation is performed from n = 1.20-1.30, and the refractive index change step is 0.02. As shown in Figure 8(a), the minimum frequency position of the transmission spectrum shows a red shift as the

TABLE 1. Performance comparison reported in various THz metamaterial sensors.

	Sensitivity (GHz/RIU)	Q-factor	FoM(THz)	Analyte thickness
This work	930.4	23.7	12.53	50μm
Ref[18]	788	20	-	30μm
Ref[47]	300	22.05	0.102	-
Ref[48]	163	7.036	0.061	-
Ref[49]	66	-	-	10μm

refractive index increases. The fitting curve of the refractive index sensing is shown in Figure 8(b). It is observed that the fitted curve is not a straight line, which is a common case that has been proven. However, the value of the red shift for two dips is different. A large red shift occurs at higher frequencies. As mentioned above, the reason is that the lower ring unit introduces considerable power loss due to the presence of the substrate. Meanwhile, some of the energy from the lower ring can be coupled into that of the upper ring, resulting in a higher red shift of the high frequency [46].

In order to obtain in-depth insight into the mechanism leading to this superior sensitivity, three important factors were considered that are indicative of the sensor performance, namely, the refractive index sensitivity S, the figure of merit (FoM), and the Q-factor. The term S is defined as the change in the LSPR wavelength ($\Delta\lambda_{LSPR}$) per unit refractive index (RIU), as shown in Eq. 5. The FoM is defined as the ratio between the S and the full width at half maximum (FWHM) centered at the resonance wavelength, as shown in Eq. 6. Q is defined as the ratio between the λ and FWHM centered at the resonance wavelength, as shown in Eq. 7.

$$S = \Delta\lambda_{LSPR}\big/\Delta n \qquad (5)$$
$$FoM = S\big/FWHM \qquad (6)$$
$$Q = \lambda\big/FWHM \qquad (7)$$

As shown in Figure 8(b), the highest sensitivity of the SDSRR structure is calculated to be 930.4 GHz/RIU, and the refractive index of the surrounding medium varies from 1.0 to 1.3. This result exceeds the performance of similar reported metamaterial sensors based on the same waveband, as shown in Table 1. All these data show that in THz sensing applications, the sensitivity of SDSRR is significantly better than other planar structures (maximum sensitivity around 300 GHz/RIU) and other vertical structures (maximum sensitivity around 800 GHz/RIU). Small biomolecules with thickness up to 50 μm, such as fungal bacteria, or some biomacromolecules such as DNA or proteins have refractive indices in the range of 1.1-1.6. Therefore, highly sensitive detection and discrimination of biomolecules can be achieved. Even when the change in refractive index is only 0.01, it can be accurately detected.

IV. CONCLUSION

This paper proposes a dual-band stereo metamaterial sensor based on coupling electrical resonance and magnetic resonance. This design, which introduces stronger resonances, can not only greatly improve the sensitivity for a wide incidence angle up to 50°, but can also independently tune each dip by changing the size of the structure within a smaller range. In particular, due to strong resonance, the SDSRR sensor can still maintain its excellent sensing feature when the analyte thickness reaches 50 μm. For these reasons, the SDSRR sensor performs much better than other vertical metamaterial sensors. Although the vertical SRR structures had been analyzed, fabricated, and presented by several groups [50]–[56], the complexity of vertical metamaterial structure and our limited processing conditions lead to a lack of test results. An assumption for SDSRR structure processing is introduced in the Supplementary documentation, but future studies will need to verify this processing. Even so, this sensor design methodology has practical guidance implications and broad application prospects in biomolecule detection and discrimination.

REFERENCES

[1] M. Zhang and J. T. W. Yeow, "Nanotechnology-based terahertz biological sensing: A review of its current state and things to come," *IEEE Nanotechnol. Mag.*, vol. 10, no. 3, pp. 30–38, Sep. 2016.

[2] K. Shih, P. Pitchappa, L. Jin, C. Chen, R. Singh, and C. Lee, "Nanofluidic terahertz metasensor for sensing in aqueous environment," *Appl. Phys. Lett.*, vol. 113, no. 7, p. 71105, 2018.

[3] K. V. Sreekanth, Y. Alapan, M. ElKabbash, E. Ilker, M. Hinczewski, U. A. Gurkan, A. De Luca, and G. Strangi, "Extreme sensitivity biosensing platform based on hyperbolic metamaterials," *Nature Mater.*, vol. 15, no. 6, pp. 621–627, Jun. 2016.

[4] Y. Ryu, D. Lee, J. Kang, S. Lee, E. Yu, and M. Seo, "Ultrasensitive terahertz sensing of gold nanoparticles inside nano slot antennas," *Opt. Exp.*, vol. 25, no. 24, pp. 30591–30597, 2017.

[5] Y. Liu and X. Zhang, "Metamaterials: A new frontier of science and technology," *Chem. Soc. Rev.*, vol. 40, no. 5, pp. 2494–2507, Jan. 2011.

[6] J. B. Pendry, A. J. Holden, W. J. Stewart, and I. Youngs, "Extremely low frequency plasmons in metallic mesostructures," *Phys. Rev. Lett.*, vol. 76, no. 25, pp. 4773–4776, Jun. 1996.

[7] R. Marqués, J. Martel, F. Mesa, and F. Medina, "Left-Handed-Media simulation and transmission of EM waves in subwavelength Split-Ring-Resonator-Loaded metallic waveguides," *Phys. Rev. Lett.*, vol. 89, no. 18, Oct. 2002, Art. no. 183901.

[8] Z. G. Dong, S. N. Zhu, H. Liu, J. Zhu, and W. Cao, "Numerical simulations of negative-index refraction in wedge-shaped metamaterials," *Phys. Rev. E, Stat. Phys. Plasmas Fluids Relat. Interdiscip. Top.*, vol. 72, no. 1, p. 16607, Jul. 2005.

[9] S. Tan, F. Yan, L. Singh, W. Cao, N. Xu, X. Hu, R. Singh, M. Wang, and W. Zhang, "Terahertz metasurfaces with a high refractive index enhanced by the strong nearest neighbor coupling," *Opt. Exp.*, vol. 23, no. 22, p. 29222, 2015.

[10] Z. Geng, X. Zhang, Z. Fan, X. Lv, and H. Chen, "A route to terahertz metamaterial biosensor integrated with microfluidics for liver cancer biomarker testing in early stage," *Sci. Rep.*, vol. 7, no. 1, p. 16378, Dec. 2017.

[11] D.-K. Lee, J.-H. Kang, J. Kwon, J.-S. Lee, S. Lee, D. H. Woo, J. H. Kim, C.-S. Song, Q.-H. Park, and M. Seo, "Nano metamaterials for ultrasensitive terahertz biosensing," *Sci. Rep.*, vol. 7, no. 1, p. 8146, Dec. 2017.

[12] J. Zhu, S. Li, L. Deng, C. Zhang, Y. Yang, and H. Zhu, "Broadband tunable terahertz polarization converter based on a sinusoidally-slotted graphene metamaterial," *Opt. Mater. Exp.*, vol. 8, no. 5, p. 1164, 2018.

[13] L. Nama, S. Bhattacharyya, and P. Chakrabarti, "A metasurface-based broadband quasi nondispersive cross polarization converter for far infrared region," *J. RF Microw. Comput.-Aided Eng.*, vol. 29, no. 10, 2019, Art. no. e21889.

[14] S. K. Ghosh, V. S. Yadav, S. Das, and S. Bhattacharyya, "Tunable graphene-based metasurface for polarization-independent broadband absorption in lower mid-infrared (MIR) range," *IEEE Trans. Electromagn. Compat.*, vol. 62, no. 2, pp. 346–354, Apr. 2020.

[15] Y. Yang, D. Xu, and W. Zhang, "High-sensitivity and label-free identification of a transgenic genome using a terahertz meta-biosensor," *Opt. Exp.*, vol. 26, no. 24, p. 31589, 2018.

[16] Y. K. Srivastava, L. Cong, and R. Singh, "Dual-surface flexible THz fano metasensor," *Appl. Phys. Lett.*, vol. 111, no. 20, Nov. 2017, Art. no. 201101.

[17] T. Chen, S. Li, and H. Sun, "Metamaterials application in sensing," *Sensors*, vol. 12, no. 3, pp. 2742–2765, Feb. 2012.

[18] W. Wang, F. Yan, S. Tan, H. Zhou, and Y. Hou, "Ultrasensitive terahertz metamaterial sensor based on vertical split ring resonators," *Photon. Res.*, vol. 5, no. 6, p. 571, 2017.

[19] S. Luo, B. Li, A. Yu, J. Gao, X. Wang, and D. Zuo, "Broadband tunable terahertz polarization converter based on graphene metamaterial," *Opt. Commun.*, vol. 413, pp. 184–189, Apr. 2018.

[20] V. S. Yadav, S. K. Ghosh, S. Das, and S. Bhattacharyya, "Wideband tunable mid-infrared cross-polarisation converter using monolayered graphene-based metasurface over a wide angle of incidence," *IET Microw., Antennas Propag.*, vol. 13, no. 1, pp. 82–87, Jan. 2019.

[21] L. Cong, S. Tan, R. Yahiaoui, F. Yan, W. Zhang, and R. Singh, "Experimental demonstration of ultrasensitive sensing with terahertz metamaterial absorbers: A comparison with the metasurfaces," *Appl. Phys. Lett.*, vol. 106, no. 3, p. 31107, 2015.

[22] L. Yang, T. Guo, X. Zhang, S. Cao, and X. Ding, "Toxic chemical compound detection by terahertz spectroscopy: A review," *Rev. Anal. Chem.*, vol. 37, no. 3, p. 2018, Sep. 2018.

[23] J. B. Pendry, A. J. Holden, D. J. Robbins, and W. J. Stewart, "Magnetism from conductors and enhanced nonlinear phenomena," *IEEE Trans. Microw. Theory Techn.*, vol. 47, no. 11, pp. 2075–2084, Nov. 1999.

[24] J. Wang, C. Fan, J. He, P. Ding, E. Liang, and Q. Xue, "Double Fano resonances due to interplay of electric and magnetic plasmon modes in planar plasmonic structure with high sensing sensitivity," *Opt. Exp.*, vol. 21, no. 2, pp. 2236–2244, 2013.

[25] W. Xu, L. Xie, and Y. Ying, "Mechanisms and applications of terahertz metamaterial sensing: A review," *Nanoscale*, vol. 9, no. 37, pp. 13864–13878, 2017.

[26] R. Zhou, C. Wang, W. Xu, and L. Xie, "Biological applications of terahertz technology based on nanomaterials and nanostructures," *Nanoscale*, vol. 11, no. 8, pp. 3445–3457, 2019.

[27] H. Teguh Yudistira, A. Pradhipta Tenggara, V. Dat Nguyen, T. Teun Kim, F. Dian Prasetyo, C.-G. Choi, M. Choi, and D. Byun, "Fabrication of terahertz metamaterial with high refractive index using high-resolution electrohydrodynamic jet printing," *Appl. Phys. Lett.*, vol. 103, no. 21, Nov. 2013, Art. no. 211106.

[28] X. Yan, M. Yang, Z. Zhang, T. W. Wei, L. Liu, and J. Xie, "The terahertz electromagnetically induced transparency-like metamaterials for sensitive biosensors in the detection of cancer cells," *Biosensors Bioelectron.*, vol. 126, pp. 485–492, Feb. 2019.

[29] A. Keshavarz and Z. Vafapour, "Thermo-optical applications of a novel terahertz semiconductor metamaterial design," *J. Opt. Soc. Amer. B, Opt. Phys.*, vol. 36, no. 1, p. 35, 2019.

[30] P. C. Wu, W. T. Chen, K.-Y. Yang, C. T. Hsiao, G. Sun, A. Q. Liu, N. I. Zheludev, and D. P. Tsai, "Magnetic plasmon induced transparency in three-dimensional metamolecules," *Nanophotonics*, vol. 1, no. 2, pp. 131–138, Nov. 2012.

[31] K. Fan, A. C. Strikwerda, X. Zhang, and R. D. Averitt, "Three-dimensional broadband tunable terahertz metamaterials," *Phys. Rev. B, Condens. Matter*, vol. 87, no. 16, p. 2013, Apr. 2013.

[32] P. C. Wu, G. Sun, W. T. Chen, K. Yang, Y. Huang, and Y. Chen, "Vertical split-ring resonator based nanoplasmonic sensor," *Appl. Phys. Lett.*, vol. 105, no. 3, p. 33105, 2014.

[33] X. Chen, W. Fan, and C. Song, "Multiple plasmonic resonance excitations on graphene metamaterials for ultrasensitive terahertz sensing," *Carbon*, vol. 133, pp. 416–422, Jul. 2018.

[34] J. Chen, C. Peng, S. Qi, Q. Zhang, C. Tang, X. Shen, H. Da, L. Wang, and G.-S. Park, "Photonic microcavity-enhanced magnetic plasmon resonance of metamaterials for sensing applications," *IEEE Photon. Technol. Lett.*, vol. 31, no. 2, pp. 113–116, Jan. 15, 2019.

[35] Y. Shi, Z.-Y. Li, K. Li, L. Li, and C.-H. Liang, "A retrieval method of effective electromagnetic parameters for inhomogeneous metamaterials," *IEEE Trans. Microw. Theory Techn.*, vol. 65, no. 4, pp. 1160–1178, Apr. 2017.

[36] L. L. Hou, J. Y. Chin, X. M. Yang, X. Q. Lin, R. Liu, and F. Y. Xu, "Advanced parameter retrievals for metamaterial slabs using an inhomogeneous model," *J. Appl. Phys.*, vol. 103, no. 6, p. 64904, 2008.

[37] W. B. Weir, "Automatic measurement of complex dielectric constant and permeability at microwave frequencies," *Proc. IEEE*, vol. 62, no. 1, pp. 33–36, Jan. 1974.

[38] D. R. Smith, S. Schultz, P. Markoš, and C. M. Soukoulis, "Determination of effective permittivity and permeability of metamaterials from reflection and transmission coefficients," *Phys. Rev. B, Condens. Matter*, vol. 65, no. 19, p. 2001, Apr. 2002.

[39] D. R. Smith, D. C. Vier, T. Koschny, and C. M. Soukoulis, "Electromagnetic parameter retrieval from inhomogeneous metamaterials," *Phys. Rev. E, Stat. Phys. Plasmas Fluids Relat. Interdiscip. Top.*, vol. 71, no. 3, p. 36617, Mar. 2005.

[40] M. Chen, Z. Xiao, X. Lu, F. Lv, and Y. Zhou, "Simulation of dynamically tunable and switchable electromagnetically induced transparency analogue based on metal-graphene hybrid metamaterial," *Carbon*, vol. 159, pp. 273–282, Apr. 2020.

[41] W. J. Padilla, A. J. Taylor, C. Highstrete, M. Lee, and R. D. Averitt, "Dynamical electric and magnetic metamaterial response at terahertz frequencies," *Phys. Rev. Lett.*, vol. 96, no. 10, Mar. 2006, Art. no. 107401.

[42] T. Driscoll, G. O. Andreev, D. N. Basov, S. Palit, S. Y. Cho, and N. M. Jokerst, "Tuned permeability in terahertz split-ring resonators for devices and sensors," *Appl. Phys. Lett.*, vol. 91, no. 6, 2007, Art. no. 062511.

[43] N. Katsarakis, T. Koschny, M. Kafesaki, E. N. Economou, and C. M. Soukoulis, "Electric coupling to the magnetic resonance of split ring resonators," *Appl. Phys. Lett.*, vol. 84, no. 15, pp. 2943–2945, Apr. 2004.

[44] K. Fan, A. C. Strikwerda, H. Tao, X. Zhang, and R. D. Averitt, "Stand-up magnetic metamaterials at terahertz frequencies," *Opt. Exp.*, vol. 19, no. 13, pp. 12619–12627, 2011.

[45] R. Marqués, F. Medina, and R. Rafii-El-Idrissi, "Role of bianisotropy in negative permeability and left-handed metamaterials," *Phys. Rev. B, Condens. Matter*, vol. 65, no. 14, Apr. 2002, Art. no. 144440.

[46] A. Dmitriev, C. Hägglund, S. Chen, H. Fredriksson, T. Pakizeh, M. Käll, and D. S. Sutherland, "Enhanced nanoplasmonic optical sensors with reduced substrate effect," *Nano Lett.*, vol. 8, no. 11, pp. 3893–3898, Nov. 2008.

[47] A. S. Saadeldin, M. F. O. Hameed, E. M. A. Elkaramany, and S. S. A. Obayya, "Highly sensitive terahertz metamaterial sensor," *IEEE Sensors J.*, vol. 19, no. 18, pp. 7993–7999, Sep. 2019.

[48] L. Cong and R. Singh, "Sensing with THz metamaterial absorbers," 2014, *arXiv:1408.3711*. [Online]. Available: http://arxiv.org/abs/1408.3711

[49] M. S. Islam, J. Sultana, M. Biabanifard, Z. Vafapour, M. J. Nine, and A. Dinovitser, "Tunable localized surface plasmon graphene metasurface for multiband superabsorption and terahertz sensing," *Carbon*, vol. 158, pp. 559–567, Mar. 2020.

[50] Q. Meng, Z. Zhong, and B. Zhang, "Hybrid three-dimensional dual- and broadband optically tunable terahertz metamaterials," *Sci. Rep.*, vol. 7, no. 1, p. 45708, May 2017.

[51] W. T. Chen, C. J. Chen, P. C. Wu, S. Sun, L. Zhou, G.-Y. Guo, C. T. Hsiao, K.-Y. Yang, N. I. Zheludev, and D. P. Tsai, "Optical magnetic response in three-dimensional metamaterial of upright plasmonic meta-molecules," *Opt. Exp.*, vol. 19, no. 13, p. 12837, 2011.

[52] P. C. Wu, W.-L. Hsu, W. T. Chen, Y.-W. Huang, C. Y. Liao, A. Q. Liu, N. I. Zheludev, G. Sun, and D. P. Tsai, "Plasmon coupling in vertical split-ring resonator metamolecules," *Sci. Rep.*, vol. 5, no. 1, p. 9726, Sep. 2015.

[53] D. Liang, H. Zhang, J. Gu, Y. Li, Z. Tian, C. Ouyang, J. Han, and W. Zhang, "Plasmonic analog of electromagnetically induced transparency in stereo metamaterials," *IEEE J. Sel. Topics Quantum Electron.*, vol. 23, no. 4, pp. 1–7, Jul. 2017.

[54] K. Fan, A. C. Strikwerda, H. Tao, X. Zhang, and R. D. Averitt, "Stand-up magnetic metamaterials at terahertz frequencies," *Opt. Exp.*, vol. 19, no. 13, p. 12619, 2011.

[55] P. C. Wu, G. Sun, W. T. Chen, K. Yang, Y. Huang, and Y. Chen, "Vertical split-ring resonator based nanoplasmonic sensor," *Appl. Phys. Lett.*, vol. 105, no. 3, 2014, Art. no. 033105.

PENGFEI CAO received the Ph.D. degree from Lanzhou University, Lanzhou. He is currently an Associate Professor with Lanzhou University. He has published more than 20 papers in journals and international refereed conferences. His research interests include terahertz metamaterial and terahertz sensing technology.

JING ZHANG received the bachelor's degree from Chang'an University, Xi'an, where she is currently pursuing the master's degree. Her research interests include terahertz metamaterial and terahertz sensing technology.
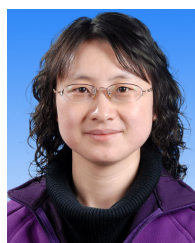
YUYAO WU received the bachelor's degree from the Lanzhou University of Technology, Lanzhou, where he is currently pursuing the master's degree. His research interests include terahertz metamaterial and terahertz sensing technology.

QIANG LIU received the bachelor's degree from Yan'an University, and the master's degree from the Nanjing University of Technology. He is currently working for Northwest Industries Group Company Ltd., CN. His research interests include terahertz metamaterial and terahertz sensing technology.

ZELONG WANG received the master's degree from Lanzhou University. He is currently pursuing the Ph.D. degree with Tianjin University. His research interests include terahertz metamaterial and terahertz sensing technology.

LIN CHENG received the Ph.D. degree from Lanzhou University, Lanzhou. She is currently an Associate Professor with Lanzhou University. She has published more than 20 papers in journals and international refereed conferences. Her research interests include terahertz metamaterial and terahertz imaging technology.

YUAN LI received the bachelor's degree from the Xi'an University of Technology, Xi'an, where he is currently pursuing the master's degree. His research interests include terahertz metamaterial and terahertz sensing technology.
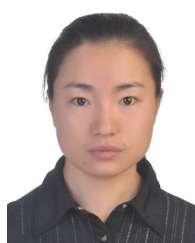
TIAOMING NIU received the Ph.D. degree from The University of Adelaide, Australia. She is currently a Lecturer with Lanzhou University, Lanzhou. She has published more than ten papers in journals and international refereed conferences. Her research interests include terahertz metamaterial and terahertz antenna technology.

• • •